



Dye-sensitized solar cells achieved with multi-layered SnO₂/ZnO composite photoanodes through precise control of

Downloaded from: <https://research.chalmers.se>, 2025-02-23 05:33 UTC


Citation for the original published paper (version of record):

Weerasinghe, M., Kumarasinghe, K., Karunaratne, B. et al (2024). Dye-sensitized solar cells achieved with multi-layered SnO₂/ZnO composite photoanodes through precise control of thickness and composition. *Journal of Materials Science: Materials in Electronics*, 35(33). <http://dx.doi.org/10.1007/s10854-024-13837-1>

N.B. When citing this work, cite the original published paper.



Dye-sensitized solar cells achieved with multi-layered SnO₂/ZnO composite photoanodes through precise control of thickness and composition

M. I. U. Weerasinghe^{1,2}, K. D. M. S. P. K. Kumarasinghe¹, Buddhika C. Karunaratne¹, P. M. L. Kumarage¹, T. M. W. J. Bandara^{2,3}, Kirithi Tennakone¹, I. Albinsson⁴, B. E. Mellander^{5,*} , and G. R. A. Kumara^{1,*}

¹ National Institute of Fundamental Studies, Hantana Road, Kandy 20000, Sri Lanka

² Postgraduate Institute of Science, University of Peradeniya, Peradeniya 20400, Sri Lanka

³ Department of Physics, Faculty of Science, University of Peradeniya, Peradeniya 20400, Sri Lanka

⁴ Department of Physics, University of Gothenburg, Gothenburg, Sweden

⁵ Department of Physics, Chalmers University of Technology, Gothenburg, Sweden

Received: 15 August 2024

Accepted: 2 November 2024

Published online:

18 November 2024

© The Author(s), 2024

ABSTRACT

The spin coating is cost-effective, straightforward, and highly suitable for the large-scale production of solar cells. In this study, we report the fabrication of SnO₂/ZnO composite films for dye-sensitized solar cells (DSCs) using a simplified and cost-effective spin-coating technique on fluorine-doped tin oxide glass substrates. This study introduces a new way of preparing a multi-layered composite thin film using a suspension containing colloidal SnO₂ nanoparticles and ZnO nanoparticles followed by sonication and aging of TiO₂-free high-efficiency DSCs. Our approach provides a facile way of obtaining a uniform film of tunable thickness with high reproducibility by adjusting the total number of coating cycles. The spin-coating process achieved a nano-sized SnO₂-covered ZnO layer, contributing to enhanced conversion efficiency in DSCs. A specific number of seven coating cycles was identified as optimal for achieving the aspirational performance. Under standard AM 1.5 irradiation with an intensity of 100 mW/cm², the fabricated SnO₂/ZnO composite films revealed an overall energy conversion efficiency of 6.5% with a thickness of 2.06 μm which is impressive for a TiO₂-free DSC. This achievement indicates the potential of the developed fabrication process for cost-effective and scalable production of efficient DSCs with SnO₂/ZnO composite.

Address correspondence to E-mail: f5xrk@chalmers.se; grakumara2000@yahoo.com

1 Introduction

During the past decade, solar cell electricity production has experienced an average annual economic growth rate of more than 34%, making it the fastest advancing energy conversion technology in the world [1]. While first- and second-generation solar cells are commercially available, comprehensive research has been conducted to develop third-generation photovoltaic devices, especially dye-sensitized solar cells (DSCs), due to their potential for high-efficiency outdoor applications [2, 3]. DSCs offer flexibility in terms of size, color, and shape and their higher efficiency at low-light illumination makes them suitable for various environments and indoor applications [4–6]. However, further research is needed to enhance the efficiency and stability of DSCs, particularly by exploring new materials and synthesis methods, to make them commercially viable [7].

The most critical component of a DSC is the photoanode, which generates photoelectrons by harnessing visible light photons. Extensive research has been conducted on titanium dioxide (TiO_2)-based photoelectrodes for DSCs since the ground-breaking invention by O'Regan and Grätzel [2, 6]. While TiO_2 has shown state-of-the-art efficiencies in DSCs, porous films made from high band gap semiconductors, aside from TiO_2 , can also facilitate dye sensitization. Therefore, solar cells made solely from alternative materials such as zinc oxide (ZnO), tin oxide (SnO_2), and niobium pentoxide (Nb_2O_5) have also been investigated to enhance the efficiency of dye-sensitized photoelectrochemical cells [2, 8–13]. However, DSCs fabricated from those oxides yield significantly lower values of efficiency compared to those based on TiO_2 photoanode due to the rapid recombination of injected dye cations with the conduction band of the semiconductor [14]. Combining semiconductors with different band gaps can reduce electron recombination and improve the power conversion efficiency (PCE) of DSCs. In 1998, Kirthi Tennakone and colleagues first demonstrated that composite films of SnO_2/ZnO could serve as effective photoanodes in the dye-sensitized solar cells, achieving a notable efficiency of 8% under an illumination intensity of 900 W m^{-2} [15]. Their research also explored various other composite films incorporating SnO_2 , including $\text{SnO}_2/\text{CaCO}_3$ [16], $\text{SnO}_2/\text{Al}_2\text{O}_3$ [17], and SnO_2/MgO [18, 19]. Among these, the SnO_2/ZnO composite film-based DSCs garnered significant attention due to their superior energy conversion efficiencies. This interest can be

attributed to the inherent properties of ZnO and SnO_2 , such as low electrical resistivity and high transparency within the visible spectrum, facilitated by their extensive bandgaps [20, 21]. The choice of appropriate thin-film fabrication methods is crucial to increase the optical and structural properties of the photoanode, methods like spray pyrolysis, screen printing, spin coating, and sputtering. Among those fabrication techniques spray pyrolysis, screen printing, and sputtering have been used to prepare SnO_2/ZnO composite films [8, 14, 20]. To the best of our knowledge, this is the first time SnO_2/ZnO composite films were prepared using the spin-coating method. In addition, the present approach offers a straightforward method to achieve uniformly thick films of SnO_2/ZnO composite that can be tuned according to the requirements of applications. The thickness of these uniform films is highly reproducible and can be controlled by adjusting the total number of coating cycles.

Spin coating is a widely used technique in fabricating thin films, particularly for the DSCs. This method is favored for its simplicity, efficiency, and ability to produce uniform coatings over large areas compared to other coating techniques. It involves depositing a small amount of suspension, containing the coating material, on to the center of a substrate, subsequently, the substrate is rotated at high speed allowing the solution to spread outward due to centrifugal force. Consequently, spin coating is a cost-effective and scalable thin-film deposition process that allows for precise control over film properties by adjusting the precursor solution composition, spin speed, and the number of coating cycles [22, 23]. It provides better wetting and adhesion between absorbent layers and Fluorine-doped Tin Oxide (FTO) glass substrate, resulting in minor defects at the interfaces. This is important to minimize the energy barriers which is correlated with impeding charge transport [24].

In this study, highly porous SnO_2/ZnO films were deposited on FTO glass substrates using the spin-coating method. Different layer thicknesses of the photoanode were achieved by varying the number of cycles, and the amount of ZnO in the precursor solution was optimized to achieve highly efficient DSCs.

2 Experimental section

Initially, fluorine-doped tin oxide (FTO) plates ($1.5 \text{ cm} \times 2 \text{ cm}$) were cleaned by ultra-sonication in a detergent for 15 min and thoroughly washed with distilled

water. Then, these clean glass substrates were rinsed with isopropyl alcohol and dried using dry air. Also, commercially available chemicals of purity 98% or more were used to prepare samples without further purification.

The procedure followed to prepare the nanocrystalline SnO_2/ZnO composite, SnO_2 , and ZnO precursor solutions is already published [14]. Colloidal tin oxide (3 ml, 15% aqueous dispersion, Alfa Aesar), glacial acetic acid (6 drops), and ZnO (0.10-g Aldrich, particle size 30 nm) were ground in a mortar. Then Triton X-100 (5 drops) and ethanol (10 ml) were added to the paste and the suspension was sonicated for 10 min. The prepared solution was aged in a sterile environment at room temperature for about 24 h. After aging, the resultant solution was stirred at 40 °C for 15 min at 400 rpm.

The suspension was spin-coated onto cleaned FTO substrates pre-heated to 120 °C. The above procedure was repeated by changing the total number of coating cycles, ranging from 3 to 10 coating cycles. After optimizing the number of coating cycles, the amount of ZnO in the precursor solution was changed from 0.06 to 0.20 g by increasing in steps of 0.02 g per sample. Finally, the resulting composite films were sintered at 500 °C for 30 min and cooled down to 80 °C. Figure 1 (ai) and (aii) shows the observation of transparency of the spin-coated SnO_2/ZnO composite film.

To compare and analyze the performance of the SnO_2/ZnO composite cell, we constructed two separate

control cells: one with only SnO_2 and another with only ZnO . The bare SnO_2 working electrode was prepared without any ZnO powder, while the bare ZnO electrode was made without the SnO_2 precursor solution. For each type of photoanode, we conducted measurements on three sets of solar cells to ensure reliable results. The average values of photovoltaic parameters from these measurements have been compiled and reported.

Substrates coated with films were immersed in a 0.3-mM solution of N719 dye in a 1:1 v/v tert-butanol–acetonitrile-mixed solution overnight. For the assembling of the cell, the platinum-sputtered counter electrode was clipped gently to the dye-absorbed composite surface (Fig. 1b) and the electrolyte solution (0.6-M dimethylpropyl imidazolium iodide, 0.1-M LiI, 0.05-M I_2 , 0.5-M 4-tertbutylpyridine in acetonitrile) was dropped into the space between the two electrodes. A mask with a window of 0.20 cm [2] was pasted on the photoelectrode and current–voltage characteristics were recorded using simulated irradiation using a SPD SS-25 LED Solar Simulator and VK-PA-300 K PV Power Analyzer (AM 1.5 AT 100 mW cm^{-2}). Incident photon-to-current efficiency (IPCE) and electrochemical impedance spectroscopy (EIS) measurements were taken using a Bentham TMc300 monochromator and Metrohm Autolab Potentiostat/Galvanostat Electrochemical Analyzer. Composite film morphology was examined by scanning electron microscopy (SEM, Zeiss EVO LS15).

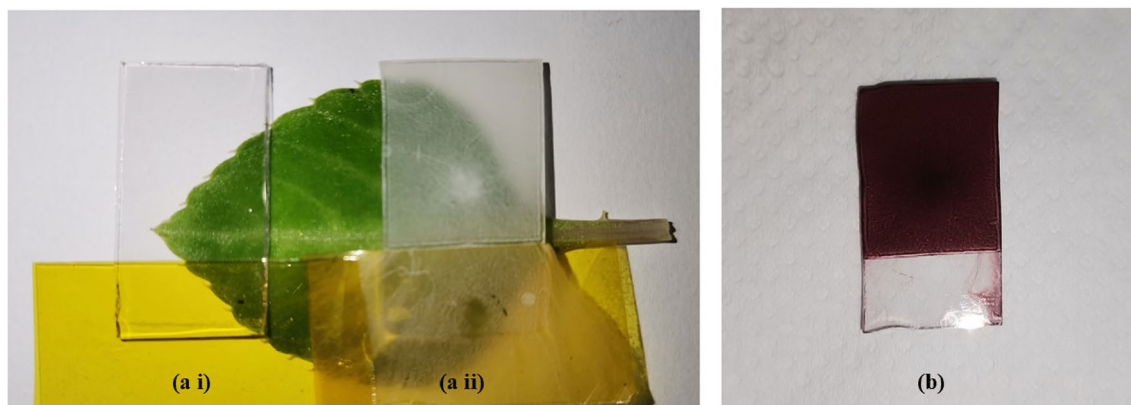


Fig. 1 Demonstration of the transparency of composite film, **a i** FTO substrate before coating, **a** optimized SnO_2/ZnO layer on the FTO substrate with seven-layer coating cycles, and **b** dye-absorbed photoanode

3 Results and discussion

3.1 SEM analysis of SnO₂/ZnO layers

Figure 2 presents the SEM images of the spin-coated composite thin films on FTO glasses, which were made by varying numbers of coating cycles. The SEM image of the SnO₂/ZnO layer, which underwent three spin-coating cycles and was thermally treated at 500 °C, is shown in Fig. 2a. In this SnO₂/ZnO composite film, clusters of SnO₂ nanoparticles coated with ZnO are observed. The surface of this layer is flat but exhibits numerous cracks. According to transverse SEM, the thickness of the layer is approximately 1.00 µm. The cracks appear to be the result of thermal stress or thermal expansion due to the energy absorbed by the nanoparticles. Moreover, during the spinning process, the nanoparticles distribute evenly across the surface due to the centrifugal force. Figure 2b depicts the SEM micrograph of the composite film prepared with 7 coating cycles. It can be seen that the cracks

in this figure have been reduced and the film surface morphology is now more compact. With further coating, the suspension onto the FTO substrate was not evenly spread and the surface became denser (Fig. 2c, layer with 10 coating cycles). It can be concluded that increasing the total number of coating cycles beyond the optimum point results in a decrease in the interconnections or interlayer bonding between layers. Also, the surface became erratic and was easily removed. In contrast, the homogeneity of films that are produced by spin coating leads to uniform electrical properties across the active area of the solar cell and a smoother surface allows better contact between the SnO₂/ZnO composite and the FTO substrate, which reduces the recombination losses and improves the charge transfer efficiency of the composite film [25, 26]. The SEM image of the cross-section of the composite layer with 7 coating cycles is shown in Fig. 2d. The layers of the seven stacks are tightly bound as shown in the cross-sectional SEM image and the estimated thickness of the seven layers is 2.06 µm.

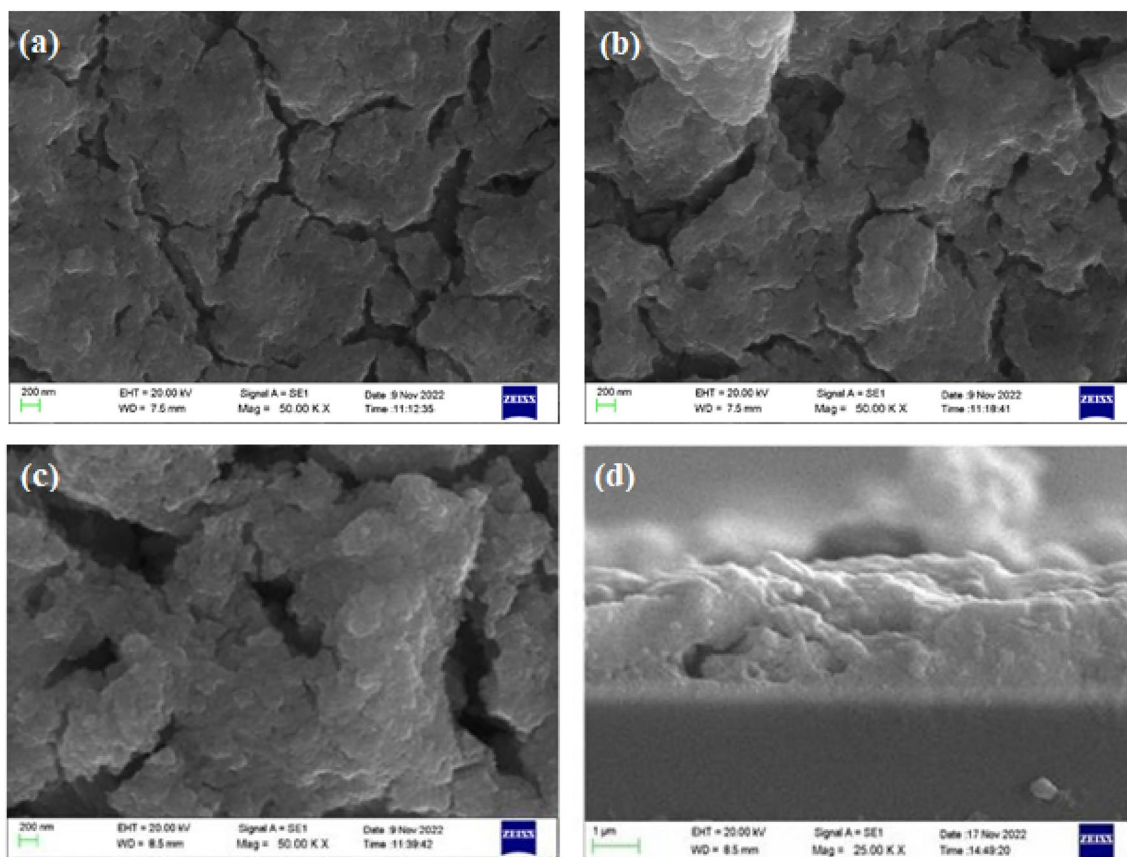


Fig. 2 The SEM images of SnO₂/ZnO layers with the total number of coating cycles at constant composition of the SnO₂/ZnO suspension, **a** 3, **b** 7 (Best efficiency), and **c** 10 on FTO glass substrates. **d** A cross-sectional image of 7 coating cycles of sample

3.2 Photocurrent–voltage (J – V) characteristics

3.2.1 Engineering the layer thickness

Photocurrent–voltage characteristics curves and variation of the conversion efficiency of DSCs fabricated by changing the total number of spin-coating cycles are shown in Fig. 3a and b, respectively. Interestingly, the total number of cycles of seven showed the highest efficiency of 5.31%, with a short-circuit current density (J_{SC}) of 17.62 mA cm^{-2} , open-circuit voltage (V_{OC}) of

0.53 V, and fill factor (FF) of 0.56 as shown in Table 1. Increasing the total number of cycles to ten attenuates the performance of DSCs.

The composite thin-film photoanode with seven coating cycles of the spin coater shows the highest short current density. This is due to the highest dye absorption of the porous SnO_2/ZnO composite layer. Further increasing the number of coating cycles after seven, the interconnections between the layers are reduced. Thus, the conversion efficiency of the composite film has decreased significantly as the total

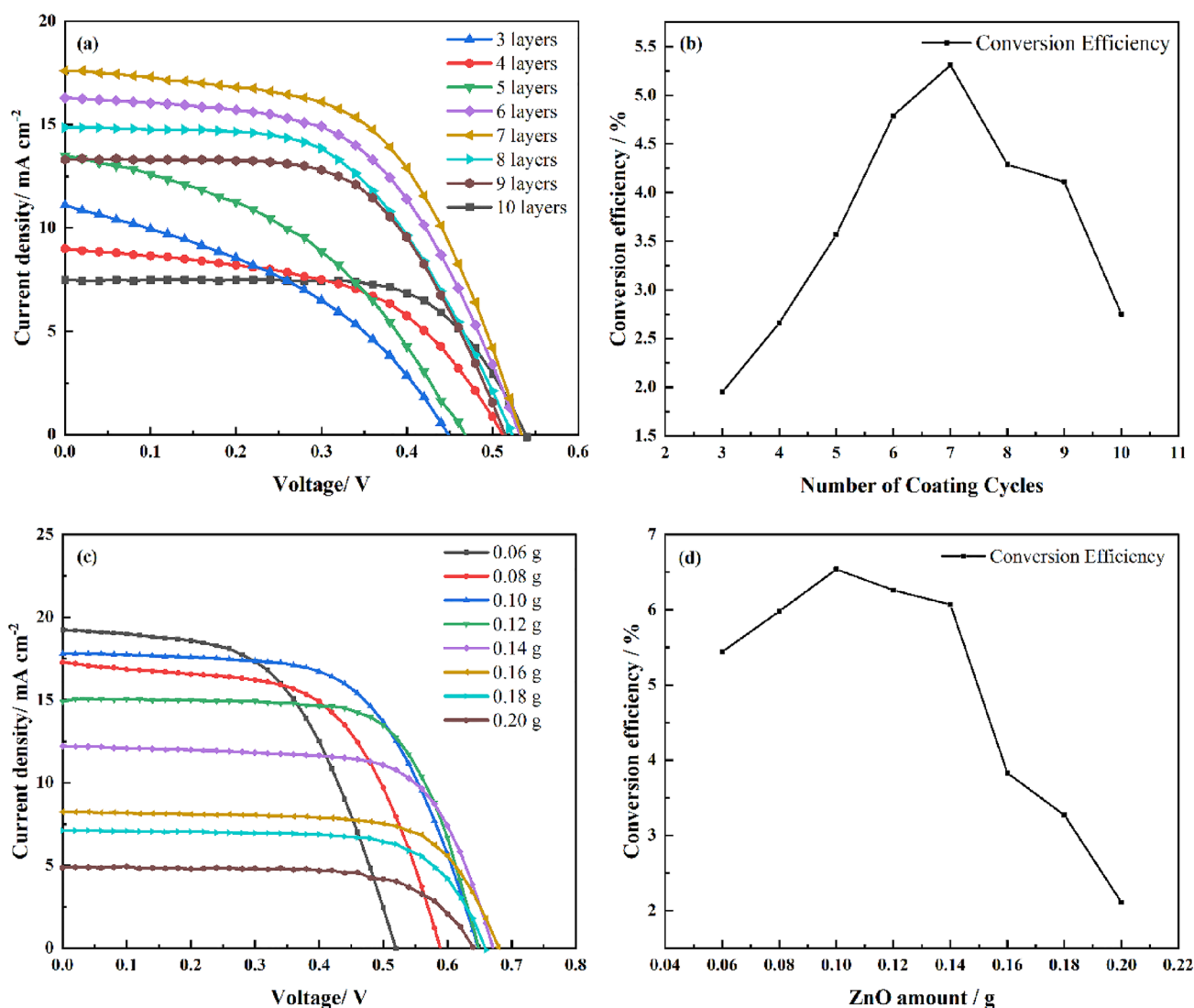


Fig. 3 **a** Current density–voltage characteristics graphs of DSCs spin-coated at the different total number of coating cycles. **b** Conversion efficiency variation of SnO_2/ZnO composite DSCs with the total number of coating cycles while maintaining the persistent composition of the composite suspension. **c** Variation

of current density–voltage characteristics graphs of DSCs made with SnO_2/ZnO composite cell with different ZnO amounts. **d** Conversion efficiency variation of DSCs with added ZnO amount in the SnO_2/ZnO photoanodes

Table 1 Photovoltaic characteristics of SnO₂/ZnO composite cells

fabricated with varying total spin-coating cycles while maintaining a constant composition of the composite suspension (0.06 g of ZnO and 3 ml of SnO₂)

No. of coating cycles	V_{oc}/V	$J_{sc}/\text{mA cm}^{-2}$	FF	$\eta/\%$
3	0.448 ± 0.004	11.1 ± 0.1	0.39 ± 0.03	1.9 ± 0.1
4	0.467 ± 0.008	13.5 ± 0.1	0.42 ± 0.01	2.7 ± 0.1
5	0.535 ± 0.001	11.9 ± 0.1	0.56 ± 0.01	3.6 ± 0.1
6	0.531 ± 0.003	16.3 ± 0.2	0.55 ± 0.00	4.8 ± 0.1
7	0.533 ± 0.003	17.6 ± 0.2	0.56 ± 0.02	5.3 ± 0.1
8	0.530 ± 0.002	14.8 ± 0.2	0.55 ± 0.01	4.3 ± 0.1
9	0.514 ± 0.002	13.3 ± 0.1	0.60 ± 0.01	4.1 ± 0.1
10	0.538 ± 0.002	7.5 ± 0.1	0.68 ± 0.04	2.8 ± 0.1

number of coating cycles of the spin coater increased after 7 cycles.

3.2.2 Optimization of ZnO content in the photoanode

The DSCs with SnO₂/ZnO composite electrodes prepared by seven coating cycles have shown superior performance according to the data given in Table 1 and Fig. 3b. Next, the suitable composition of the composite suspension is determined by varying the amount of ZnO added to the precursor mixture. The J – V curves for DSCs fabricated by varying ZnO amounts are shown in Fig. 3c and the photovoltaic parameters obtained are summarized in Table 2.

The optimum composition of ZnO in the composite paste for the highest conversion efficiency corresponds to 0.10 g as shown in Table 2. In general, photo-excited electrons are injected from the dye into the conduction band of the semiconductor. However, if the recombination of the injected electrons occurs, the cell performance is drastically reduced. The reduction of the interfacial electron recombination is responsible for

the better performance of the composite cell [14]. The efficiency variation with the ZnO amount is shown in Fig. 3c. Conversion efficiency rose as the ZnO amount increased up to 0.10 g. The presence of the ZnO forms a kind of thin-film barrier at the photo-electrode and electrolyte interface that can reduce the rate of the recombination process between interfaces and improve the device's performance. However, the graph reveals that after a certain point, the conversion efficiencies significantly decline. It is conspicuous that once the amount of ZnO approaches this threshold, the barrier becomes so strong that only extremely energetic electrons can pass into the conduction band of the oxide semiconductor. Therefore, the composite cells must include an appropriate amount of ZnO. Cells composed separately of bare SnO₂ (0.0 g of ZnO) and bare ZnO (0.0 ml of SnO₂), fabricated using a total of seven coating cycles, exhibit photovoltaic conversion efficiencies of 1.23% and 0.24%, respectively. ZnO thin films have nearly zero conversion efficiency. The reason was the inability to prepare a uniform ZnO layer by the spin-coating method, resulting in very low conversion efficiency ($V_{OC} = 0.47$ V, $J_{SC} = 1.12$ mA cm⁻²,

Table 2 Photovoltaic properties are achieved through the alteration of ZnO proportions in SnO₂/ZnO composite electrodes while maintaining the optimized number of seven coating cycles

Mass of ZnO added to 3 ml of SnO ₂ /g	V_{OC}/V	$J_{SC}/\text{mA cm}^{-2}$	FF	$\eta/\%$
0.00 (SnO ₂ only)	0.531 ± 0.002	6.4 ± 0.1	0.36 ± 0.02	1.2 ± 0.1
0.06	0.519 ± 0.002	19.2 ± 0.2	0.54 ± 0.02	5.4 ± 0.1
0.08	0.588 ± 0.003	17.3 ± 0.2	0.58 ± 0.04	5.9 ± 0.1
0.10	0.643 ± 0.001	16.4 ± 0.7	0.61 ± 0.02	6.5 ± 0.1
0.12	0.648 ± 0.002	13.9 ± 0.2	0.69 ± 0.02	6.3 ± 0.2
0.14	0.672 ± 0.001	11.3 ± 0.6	0.79 ± 0.08	6.1 ± 0.3
0.16	0.680 ± 0.001	8.2 ± 0.1	0.68 ± 0.02	3.8 ± 0.1
0.18	0.658 ± 0.001	7.1 ± 0.1	0.69 ± 0.02	3.3 ± 0.1
0.20	0.640 ± 0.003	4.9 ± 0.1	0.67 ± 0.04	2.1 ± 0.1
ZnO only	0.474 ± 0.008	1.1 ± 0.0	0.46 ± 0.01	0.2 ± 0.0

$FF = 0.46$, $\eta = 0.24\%$) of only ZnO DSCs with 7 cycles. Moreover, the poor energy conversion efficiency of the ZnO electrode may be due to the inability to aggregate dye well on the surface of the ZnO electrode [8]. In addition, the SnO_2 separate cell has lower conversion efficiency ($V_{OC} = 0.53$ V, $J_{SC} = 6.43$ mA cm⁻², $FF = 0.36$, $\eta = 1.23\%$) than the SnO_2/ZnO composite cell because the SnO_2 working electrode has a low barrier to reduce the recombination of electrons compared to the SnO_2/ZnO composite cell.

3.3 Incident photon-to-current conversion efficiency (IPCE)

The incident monochromatic photon-to-current conversion efficiency (IPCE), explained as the number of electrons generated by light in the external circuit divided by the number of incident photons, is plotted as a function of excitation wavelength [27]. IPCE spectra of the best DSC with seven cycle-coated SnO_2/ZnO photoanode, bare ZnO, and bare SnO_2 are shown in Fig. 4. The SnO_2/ZnO composite has a maximum IPCE value of 56.2% at a wavelength of 530 nm and the theoretical J_{SC} value of composite solar cell was calculated using the integrated IPCE data yielding a value of 14.4 mA/cm². The 11.3% higher experimental J_{SC} value (16.4 mA/cm²) compared to the theoretical value can be attributed to the IPCE-derived J_{SC} is a theoretical approximation based on the integration of the photon flux and device spectral response, which

might not perfectly have replicated the solar spectrum used in the J_{SC} measurement. SnO_2 and ZnO separate cells have 13.8% and 5.6% maximum IPCE values. ZnO thin films have a small IPCE value compared to others. The reason is that the seven cycle spin-coated ZnO cells did not function properly. On the other hand, the absorption band edge of the dye on the ZnO is narrow indicating that the dye aggregation is low. Also, the poor light harvesting of the dye on the SnO_2 photoanode may be due to the inability of the dye to aggregate well on the SnO_2 surface.

As shown in Fig. 4, light absorption is high on the SnO_2/ZnO photoelectrode, where the successful dye aggregation on these porous semiconductor oxide electrodes contributes to the significant light harvesting achieved by the dye.

In the SnO_2/ZnO composite cell, the larger SnO_2 particles are surrounded by smaller ZnO particles. As a result, light is absorbed by the surface of the dye-coated ZnO crystallites. The small thickness of the composite thin-film electrode with the total number of seven coating cycles (approximately 2.06 μm thickness from cross-sectional SEM image) was enough to achieve a high IPCE in the UV region because ZnO effectively absorbs UV light due to direct photo-excitation with a high absorption coefficient. In our work, the surface morphology and layer thicknesses depended on the total number of coatings of the composite film which resulted in relatively strong light absorbance.

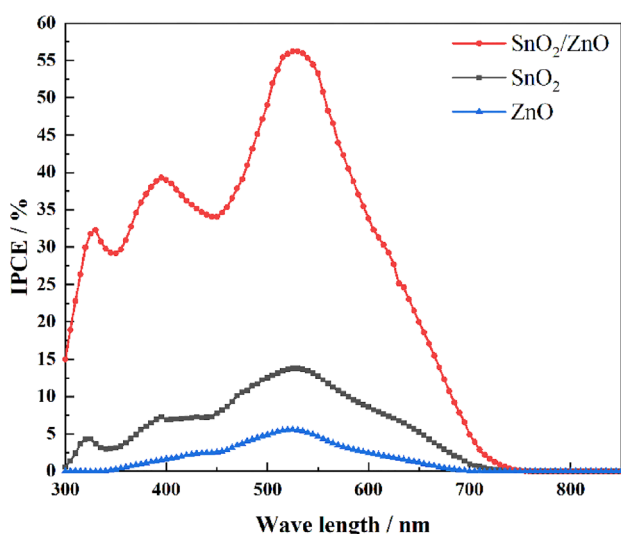


Fig. 4 IPCE graphs of seven cycle-coated thin-film DSCs prepared using optimized ZnO amount (0.10 g of ZnO) SnO_2/ZnO composite, bare SnO_2 , and bare ZnO

3.4 Electrochemical impedance spectroscopy (EIS) analysis

EIS measurements were taken to estimate the electronic and ionic properties of DSCs. The Nyquist plots for the SnO_2/ZnO , SnO_2 , and ZnO were studied. Figure 5c gives the equivalent circuit of the " $R_s + (R_{CE} || C_1) + (R_{ct} || C_2)$ " model, which has been used for representing the interface in composite solar cells. According to the equivalent circuit, parameter R_s is defined as the series resistance. R_{CE} is the charge transfer resistance of the counter electrode/electrolyte interface and the back electron transfer from FTO to the electrolyte. R_{ct} is the charge transfer resistance of the photoelectrode/electrolyte interface and the charge transport of the electrolyte. C_1 and C_2 are the capacitance at the counter electrode/electrolyte interface and photoelectrode/electrolyte interfaces, respectively.

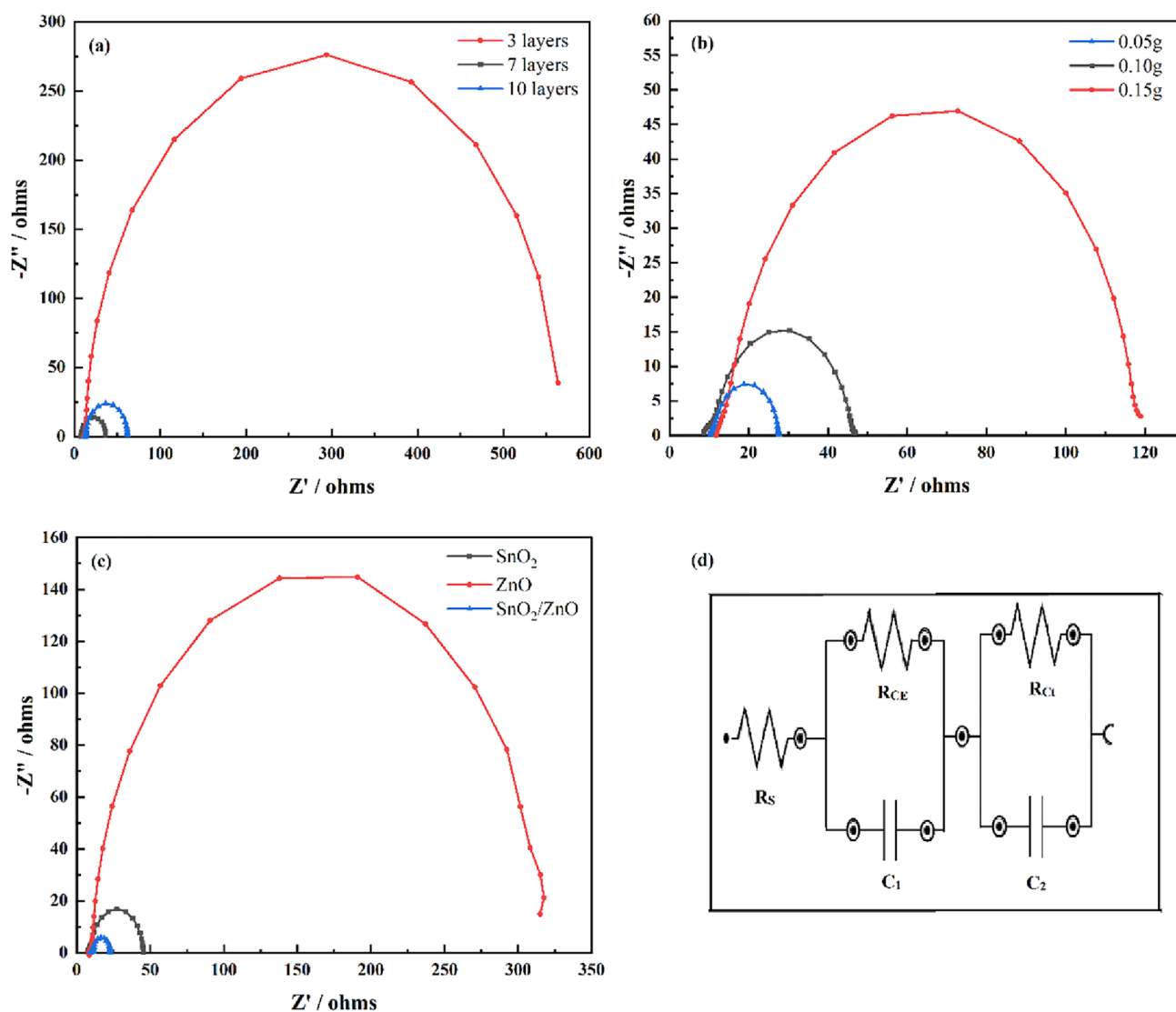


Fig. 5 EIS investigation of DSCs **a** changing the total number of coating cycles without changing the ZnO amount, **b** changing the ZnO amount of the SnO_2/ZnO composite cell, and **c** SnO_2 , ZnO, and SnO_2/ZnO separate cells prepared by coating seven total number of coating cycles. **d** The equivalent circuit model of the DSCs, in which R_s : series resistance, $C_1//R_{CE}$: charge transfer

impedance of the counter electrode/electrolyte interface and the back electron transfer from FTO to the electrolyte, and $C_2//R_{Ct}$: charge transfer impedance of the photoelectrode/electrolyte interface and the charge transport of the electrolyte measured between 1×10^{-2} and 1×10^6 Hz

The R_s is the sum of the resistance of two electrically conductive substrates and the external circuit represented by the X-axis intercept. Here, we assume that the resistance of the external circuit and the conductive (FTO) coating of the counter electrodes remain almost unchanged in the cells studied. Also, the composition of the electrolyte did not change throughout this work. The left semi-circle which corresponds to the charge transfer resistance between counter electrode/

electrolyte is invisible in most Nyquist plots. The right semi-circle which is in the low-frequency region corresponds to the charge transfer resistance at the photoanode/electrolyte of the DSC. Curves in Fig. 5 were used to extract the EIS parameters given in Table 3.

R_{CE} values of all the DSCs in this experiment near equal since the counter electrode/electrolyte interface was the same for all DSCs. As shown in Table 3a, with the three-layer count of SnO_2/ZnO , R_{Ct} gave a

Table 3 Parameters obtained by fitting the impedance data of spin-coated photoelectrode

(a) Changing the total number of coating cycles of the SnO ₂ /ZnO composite DSCs at constant composition of SnO ₂ /ZnO suspension					
Total no. of coating cycles	R_s (Ω)	R_{CE} (Ω)	R_{ct} (Ω)	τ_{ct} (s) $\times 10^{-3}$	τ_{CE} (s) $\times 10^{-5}$
3	11.4	2.32	553	1.32	-
7	7.30	1.20	28.2	1.92	3.07
10	12.2	1.48	48.3	1.32	1.45
(b) Changing the amount of ZnO of the SnO ₂ /ZnO composite DSCs at optimized total seven coating cycles					
ZnO amount (g)	R_s (Ω)	R_{CE} (Ω)	R_{ct} (Ω)	τ_{ct} (s) $\times 10^{-3}$	τ_{CE} (s) $\times 10^{-5}$
0.05	10.4	1.58	15.4	-	9.49
0.10	9.17	2.90	34.4	0.43	1.45
0.15	12.1	3.96	99.6	0.43	-
(c) Individual cells with varying photoelectrodes, all prepared using a consistent total of seven coating cycles					
Photo electrode	R_s (Ω)	R_{CE} (Ω)	R_{ct} (Ω)	τ_{ct} (s) $\times 10^{-3}$	τ_{CE} (s) $\times 10^{-5}$
Bare ZnO	10.3	7.84	297	56.6	-
Bare SnO ₂	7.71	2.14	35.1	0.14	-
SnO ₂ /ZnO	9.40	1.80	11.8	1.92	0.99

higher resistance compared to the seven- and ten-layer count, this may be due to the increased exposure of FTO to the electrolyte. The R_{ct} value is lowest for the DSC with a seven-layer count which shows the highest efficiency. This lower photoanode/electrolyte interfacial resistance shows enhanced interfacial contact due to the higher effective surface area. Further increasing in layer count to ten, increases the R_{ct} due to the bulk structure of the photoanode.

The increase in the amount of ZnO of the composite photoelectrode suspension increases the R_{ct} of DSCs drastically as shown in Fig. 5b. On the other hand, the charge transfer resistance of the counter electrode/electrolyte also increases with the increase of the ZnO amount. The reason is that the higher amount of ZnO of the photoelectrode limits the catalytic activity of the counter electrode. However, 0.05-g ZnO gives a lower performance. Thus, the composite DSCs containing 0.10-g ZnO give the best performance. Table 3b gives parameters obtained by fitting the impedance data.

Furthermore, as shown in Fig. 5c and Table 3c, the SnO₂/ZnO composite cell gives the lowest charge transfer resistance compared to the SnO₂ and ZnO separate cells. This might be due to the decreasing recombination of injected electrons of the photoelectrode/electrolyte interface by the SnO₂/ZnO composite cell. Moreover, the presence of the ZnO

in composite cells forms some kind of thin barrier at the electrode/electrolyte interface which can reduce the rate of the interfacial recombination effect.

To understand the charge transport kinetics in the nine different types of DSCs, bode phase diagrams (phase angle versus frequency plot) were used to estimate the lifetime of electrons within the SnO₂/ZnO, SnO₂, and ZnO photoanodes. The plot shows bell-shaped curves, which are symmetrical around the respective resonant frequencies [28]. Figure 6 shows the Bode phase plots of all DSCs related to this study.

Peaks (i.e., the characteristic frequencies) in the Bode phase plots represent electron lifetimes (mid-frequency range). The experimental electron lifetime related to counter electrode/electrolyte charge transfer (τ_{CE}) and photoelectrode/electrolyte interface charge transfer (τ_{ct}) can be found by the following equations: [28, 29]

$$\tau_{CE} = 1/2\pi f_{CE,max},$$

$$\tau_{ct} = 1/2\pi f_{ct,max}.$$

where $f_{CE,max}$ and $f_{ct,max}$ peaks correspond to the lifetime related to counter electrode/electrolyte charge transfer and photoelectrode/electrolyte charge transfer at the relevant frequencies. The relaxation lifetimes for the maximum frequency were calculated, and the results are shown in Table 3. Because the lifetime is

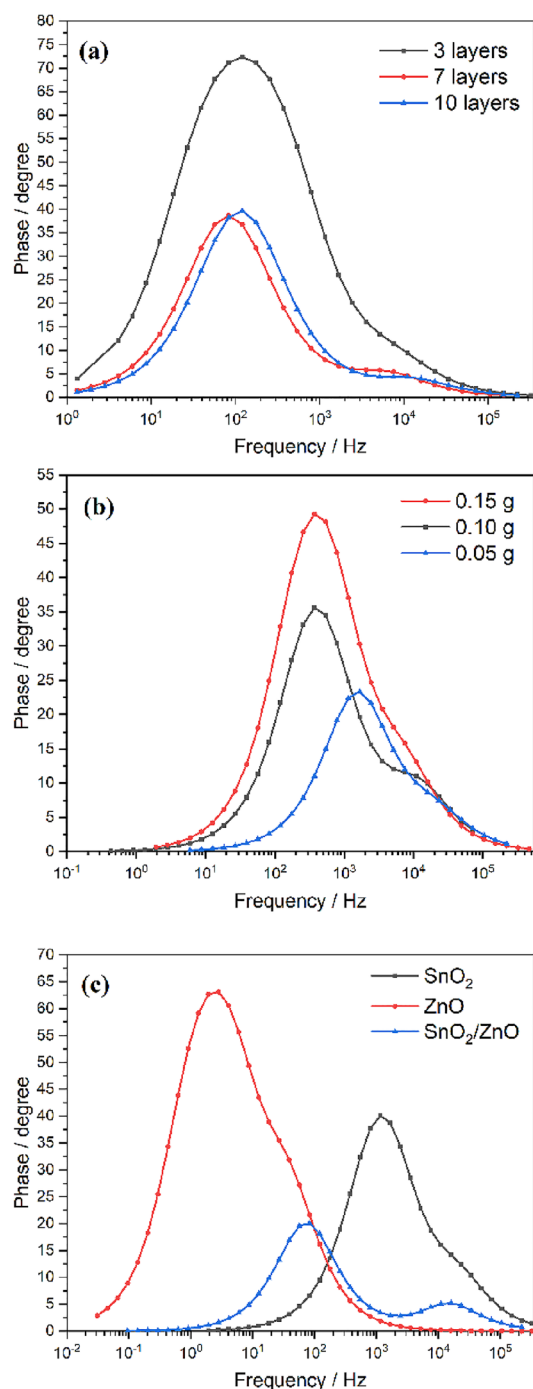


Fig. 6 Bode phase plots for EIS spectra of DSCs **a** changing the total number of coating cycles, **b** changing the ZnO amount of the SnO₂/ZnO composite cell, and **c** SnO₂, ZnO, and SnO₂/ZnO separate cells prepared by seven total coating cycles

inversely proportional to the frequency, the lower the frequency, the longer the carrier lifetime. Longer carrier and recombination lifetimes are supposed to improve DSC performance. Characteristic peak

frequencies move down with increasing film thickness, resulting in higher efficiency.

Table 3a shows that the composite photoelectrode with seven coating cycles has the highest τ_{Ct} and τ_{CE} . This indicates that it has a long carrier lifetime. Besides, as shown in Fig. 6b, τ_{Ct} does not change significantly when the amount of ZnO is increased. However, as the amount of ZnO is reduced, τ_{CE} increases. The photoanode made of 0.05 g of ZnO has the longest relaxation time, but it has a low conversion efficiency. Furthermore, the photoelectrode containing 0.10-g ZnO and prepared for the seven spin-coated cycles is the best combination.

Furthermore, different cells are prepared by changing the photoelectrode oxide semiconductor material in this work; however, only SnO₂/ZnO composite cells produce two peaks in the Bode phase graph and it indicates that electron transfer in the composite photoelectrode has achieved a faster transferring rate (Fig. 6c). The reason for this is that the recombination effect is diminishing. This result relates to the decrease in R_s , R_{CE} , and R_{Ct} which was confirmed in the EIS investigation. There is only one peak in the ZnO and SnO₂ separate cells and their conversion efficiency is lower than that of the SnO₂/ZnO composite cell. This indicates that the incorporation of SnO₂ and ZnO into photoelectrodes resulted in significant efficiency improvements due to improved light trapping and scattering in photoelectrodes. Scattering increases the chance that photons will be absorbed by the N719 sensitizer, increasing the final photocurrent yield of composite DSCs [13, 30].

In previous studies of composite dye-sensitized solar cells prepared with different types of coating methods, Kumarasinghe et al. have reported 5.04% conversion efficiency using the spray pyrolysis method [14]. Also, Masoud Abrari et al. have achieved a maximum efficiency of 3.64% for SnO₂/ZnO composite cells, which are prepared using the doctor plate method [31]. In this study, we introduced a method for preparing efficient solar cells with improved spin-coated photoanodes by depositing ultra-thin multilayers of SnO₂/ZnO composites with precise control of layer thickness and composition. The film prepared with seven coating cycles and having a layer thickness of about 2.06 μm was identified as optimal for achieving the aspirational performance. This new approach enabled achieving an efficiency of 6.5%, which is a remarkable value for TiO₂-free DSCs.

4 Conclusion

By initiating the material advantages of both SnO_2 and ZnO nanoparticles, we have achieved positive proof that an ultra-thin SnO_2/ZnO composite film solar cell prepared by spin coating yields a high conversion efficiency of 6.5%. We also optimized the total number of coating cycles and the amount of ZnO on the photoanode in this work. The optimized composite thin films show high open-circuit voltage and short current density, because the recombination of the injected electron with the dye cation is greatly suppressed. More importantly, findings demonstrate that the spin-coating technique is useful for preparing ultra-thin photo electrodes of SnO_2/ZnO composites with controlled thickness by the total number of coating cycles. In this study, a highly efficient dye-sensitized solar cell is achieved with multi-layered SnO_2/ZnO composite photoanodes through precise control of thickness and composition. This could be useful for further optimization of the electron transfer and charge recombination in highly porous composite thin-film electrodes.

Acknowledgements

This research work was fully supported by the NIFS and the University of Peradeniya, Sri Lanka.

Author contributions

M.I.U.W. contributed to Writing-original draft, Methodology, Investigation, and Formal Analysis, K.D.M.S.P.K. K. contributed to Writing-review & editing and Formal analysis, B.K. and P.M.L.K. contributed to Formal analysis and Methodology. T.M.W.J.B. contributed to Writing-review & editing and Supervision. K.T. contributed to Supervision and Writing-review and editing. I.A. and B.E.M. contributed to Formal analysis, Writing- review and editing, and Validation. G.R.A.K. contributed to Conceptualization, Supervision, and Writing-review & editing.

Funding

Open access funding provided by Chalmers University of Technology. This research work was fully

supported by the NIFS and the University of Peradeniya, Sri Lanka.

Data availability

Data will be made available on reasonable request.

Declarations

Competing interest The authors have no relevant financial or non-financial interests to disclose.

Open Access This article is licensed under a Creative Commons Attribution 4.0 International License, which permits use, sharing, adaptation, distribution and reproduction in any medium or format, as long as you give appropriate credit to the original author(s) and the source, provide a link to the Creative Commons licence, and indicate if changes were made. The images or other third party material in this article are included in the article's Creative Commons licence, unless indicated otherwise in a credit line to the material. If material is not included in the article's Creative Commons licence and your intended use is not permitted by statutory regulation or exceeds the permitted use, you will need to obtain permission directly from the copyright holder. To view a copy of this licence, visit <http://creativecommons.org/licenses/by/4.0/>.

References

1. F.R. Siegel, Access to natural resources not water or food, In: *The Earth's human carrying capacity*. Springer International Publishing: Cham **2021**, 59–70 (2020). https://doi.org/10.1007/978-3-030-73476-3_6
2. A.B. Muñoz-García, I. Benesperi, G. Boschloo, J.J. Concepcion, J.H. Delcamp, E.A. Gibson, G.J. Meyer, M. Pavone, H. Pettersson, A. Hagfeldt, M. Freitag, Dye-sensitized solar cells strike back. *Chem. Soc. Rev.* **50**(22), 12450–12550 (2021). <https://doi.org/10.1039/D0CS01336F>
3. M. Kokkonen, P. Talebi, J. Zhou, S. Asgari, S.A. Soomro, F. Elsehrawy, J. Halme, S. Ahmad, A. Hagfeldt, S.G. Hashmi, Advanced research trends in dye-sensitized solar cells. *J. Mater. Chem. A* **9**(17), 10527–10545 (2021). <https://doi.org/10.1039/D1TA00690H>

4. S.O. Abdellatif, S. Josten, A.S.G. Khalil, D. Erni, F. Marlow, Transparency and Diffused Light Efficiency of Dye-Sensitized Solar Cells: Tuning and a New Figure of Merit. *IEEE J. Photovolt.* **10**(2), 522–530 (2020). <https://doi.org/10.1109/JPHOTOV.2020.2965399>
5. R. Haridas, J. Velore, S.C. Pradhan, A. Vindhyasarumi, K. Yoosaf, S. Soman, K.N.N. Unni, A. Ajayaghosh, Indoor light-harvesting dye-sensitized solar cells surpassing 30% efficiency without co-sensitizers. *Mater. Adv.* **2**(23), 7773–7787 (2021). <https://doi.org/10.1039/D1MA00829C>
6. A. Luque, (Antonio); Hegedus (Wiley, S. Handbook of Photovoltaic Science and Engineering, 2003)
7. J.E. Ikpesu, S.E. Iyuke, M. Daramola, A.O. Okewale, Synthesis of improved dye-sensitized solar cell for renewable energy power generation. *Sol. Energy* **206**, 918–934 (2020). <https://doi.org/10.1016/j.solener.2020.05.002>
8. B. Onwona-Agyeman, M. Nakao, G. Rajanya-Asoka-Kumara, Photoelectrochemical solar cells made from SnO₂/ZnO films sensitized with an indoline dye. *J. Mater. Res.* **25**(9), 1838–1841 (2010). <https://doi.org/10.1557/JMR.2010.0235>
9. S.N.F. Zainudin, H. Abdullah, M. Markom, Electrochemical studies of tin oxide based-dye-sensitized solar cells (DSSC): a review. *J. Mater. Sci.* **30**(6), 5342–5356 (2019). <https://doi.org/10.1007/S10854-019-00929-6/METRICS>
10. R. Vittal, K.-C. Ho, Zinc oxide based dye-sensitized solar cells: a review. *Renew. Sustain. Energy Rev.* **70**, 920–935 (2017). <https://doi.org/10.1016/j.rser.2016.11.273>
11. K. Tennakone, G.K.R. Senadeera, V.P.S. Perera, I.R.M. Kottegoda, L.A.A. De Silva, Dye-sensitized photoelectrochemical cells based on porous SnO/ZnO composite and TiO films with a polymer electrolyte. *Chem. Mater.* **11**(9), 2474–2477 (1999)
12. C.S.K. Ranasinghe, E.N. Jayaweera, G.R.A. Kumara, R.M.G. Rajapakse, B. Onwona-Agyeman, A.G.U. Perera, K. Tennakone, Tin oxide based dye-sensitized solid-state solar cells: surface passivation for suppression of recombination. *Mater. Sci. Semicond. Process.* **40**, 890–895 (2015). <https://doi.org/10.1016/j.mssp.2015.07.042>
13. S. Sujinnapram, S. Moungsrijun, Additive SnO₂-ZnO composite photoanode for improvement of power conversion efficiency in dye-sensitized solar cell. *Procedia Manuf.* **2**, 108–112 (2015). <https://doi.org/10.1016/j.promfg.2015.07.019>
14. K.D.M.S.P.K. Kumarasinghe, L.A. de Silva, A.G.U. Perera, K. Tennakone, S. Dehipawala, G.R.A. Kumara, Usage of ionic liquid electrolyte in tin and zinc oxide composite dye-sensitized solar cells. *Chem. Lett.* **49**(12), 1470–1472 (2020). <https://doi.org/10.1246/cl.200535>
15. K. Tennakone, G.R.R.A. Kumara, I.R.M. Kottegoda, V.P.S. Perera, An efficient dye-sensitized photoelectrochemical solar cell made from oxides of tin and zinc. *Chem. Commun.* **1**, 15–16 (1999). <https://doi.org/10.1039/a806801a>
16. K.A.T.A. Perera, S.G. Anuradha, G.R.A. Kumara, M.L. Paranawitharana, R.M.G. Rajapakse, H.M.N. Bandara, The interconnected CaCO₃ coated SnO₂ nanocrystalline dye-sensitized solar cell with superior performance. *Electrochim. Acta* **56**(11), 4135–4138 (2011). <https://doi.org/10.1016/j.electacta.2011.01.110>
17. G.R.R.A. Kumara, K. Tennakone, V.P.S. Perera, A. Konno, S. Kaneko, M. Okuya, Suppression of recombinations in a dye-sensitized photoelectrochemical cell made from a film of tin IV oxide crystallites coated with a thin layer of aluminium oxide. *J. Phys. D* **34**(6), 868–873 (2001). <https://doi.org/10.1088/0022-3727/34/6/306>
18. K. Tennakone, J. Bandara, P. Konara, M. Bandaranayake, G. Rajanya, A. Kumara, A. Konno, Enhanced efficiency of a dye-sensitized solar cell made from MgO-coated nanocrystalline SnO₂. *Jpn. J. Appl. Phys.* **40**, 8 (2001)
19. M.K.I. Senevirathna, P.K.D.D.P. Pitigala, E.V.A. Premalal, K. Tennakone, G.R.A. Kumara, A. Konno, Stability of the SnO₂/MgO dye-sensitized photoelectrochemical solar cell. *Sol. Energy Mater. Sol. Cells* **91**(6), 544–547 (2007). <https://doi.org/10.1016/j.solmat.2006.11.008>
20. S.K. Sinha, T. Rakshit, S.K. Ray, S. Bysakh, I. Manna, Growth and low-temperature photoluminescence properties of hybrid ZnO–SnO₂ nanobelts. *Philos. Mag. Lett.* **92**(9), 469–477 (2012). <https://doi.org/10.1080/09500839.2012.687502>
21. R.A. Zargar, M.A. Bhat, I.R. Parrey, M. Arora, J. Kumar, A.K. Hafiz, Optical properties of ZnO/SnO₂ composite coated film. *Optik* **127**(17), 6997–7001 (2016). <https://doi.org/10.1016/J.IJLEO.2016.05.037>
22. A. Hosseini, K. İçli, M. Özenbaş, C. Erçelebi, Fabrication and characterization of spin-coated TiO₂ films. *Energy Procedia* **60**, 191–198 (2014). <https://doi.org/10.1016/J.EGYPRO.2014.12.332>
23. A. Merazga, F. Al-Subai, A.M. Albaradi, A. Badawi, A.Y. Jaber, A.A.B. Alghamdi, Effect of sol-gel MgO spin-coating on the performance of TiO₂-based dye-sensitized solar cells. *Mater. Sci. Semicond. Process.* **41**, 114–120 (2016). <https://doi.org/10.1016/J.MSSP.2015.08.026>
24. B. Ahmadi, M.S. Seyed Dorji, M. Kianfar, M.H. Rasoulifard, A. Ahmadi, A novel multilayer thin-film membrane with high durability: preparation, characterization performance investigation. *New J. Chem.* **46**(31), 15006–15015 (2022). <https://doi.org/10.1039/D2NJ01170K>
25. M. Yang, H.C. Kim, S.-H. Hong, Growth of ZnO nanorods on fluorine-doped tin oxide substrate without catalyst by

- radio-frequency magnetron sputtering. *Thin Solid Films* **573**, 79–83 (2014). <https://doi.org/10.1016/j.tsf.2014.11.010>
26. D.A. Keller, H.-N. Barad, E. Rosh-Hodesh, A. Zaban, D. Cahen, Can Fluorine-doped tin oxide, FTO, be more like indium-doped tin oxide, ITO? reducing FTO surface roughness by introducing additional SnO₂ coating. *MRS Commun.* **8**(3), 1358–1362 (2018). <https://doi.org/10.1557/mrc.2018.179>
27. Kumara, G.R.A., Konno, A. Development of nano-porous SnO₂/ZnO composite electrode for efficient dye-sensitized solar cell. CiNii Research. *Shizuoka University Graduate School of Electronic Science Research Report*.
28. R. Kern, R. Sastrawan, J. Ferber, R. Stangl, J. Luther, Modeling and interpretation of electrical impedance spectra of dye solar cells operated under open-circuit conditions. *Electrochim. Acta* **47**(26), 4213–4225 (2002). [https://doi.org/10.1016/S0013-4686\(02\)00444-9](https://doi.org/10.1016/S0013-4686(02)00444-9)
29. T.M.W.J. Bandara, A.M.J.S. Weerasinghe, M.A.K.L. Dissanayake, G.K.R. Senadeera, M. Furlani, I. Albins-son, B.E. Mellander, Characterization of poly (vinylidene fluoride-co-hexafluoropropylene) (PVdF-HFP) nanofiber membrane based quasi solid electrolytes and their application in a dye sensitized solar cell. *Electrochim. Acta* **266**, 276–283 (2018). <https://doi.org/10.1016/J.ELECTACTA.2018.02.025>
30. H.M. Rietveld, IUCr: a profile refinement method for nuclear and magnetic structures. *Appl Crystallogr* **2**(2), 65–71 (1969). <https://doi.org/10.1107/S00218898690006558>
31. M. Abrari, M. Ahmadi, M. Ghanaatshoar, H.R. Moazami, S.S.H. Davarani, Fabrication of dye-sensitized solar cells based on SnO₂/ZnO composite nanostructures: a new facile method using dual anodic dissolution. *J. Alloys Compd.* **784**, 1036–1046 (2019). <https://doi.org/10.1016/j.jallcom.2018.12.299>

Publisher's Note Springer Nature remains neutral with regard to jurisdictional claims in published maps and institutional affiliations.